Acta Crystallographica Section F
Structural Biology and Crystallization Communications
ISSN 1744-3091

Structure of the lamin A/C R482W mutant responsible for dominant familial partial lipodystrophy (FPLD)

Eugenia Magracheva,[a] Serguei Kozlov,[b] Colin L. Stewart,[b]‡ Alexander Wlodawer[c] and Alexander Zdanov[a]*

[a]Basic Research Program SAIC-Frederick, NCI-Frederick, Frederick, MD 21702, USA, [b]Cancer and Developmental Biology Laboratory, NCI-Frederick, Frederick, MD 21702, USA, and [c]Macromolecular Crystallography Laboratory, NCI-Frederick, Frederick, MD 21702, USA

‡ Present address: Institute of Medical Biology, 8A Biomedical Grove, Immunos, Singapore 138648, Singapore.

Correspondence e-mail: zdanov@ncifcrf.gov

Received 7 April 2009
Accepted 27 May 2009

PDB Reference: R482W mutant of lamin A/C, 3gef, r3gefsf.

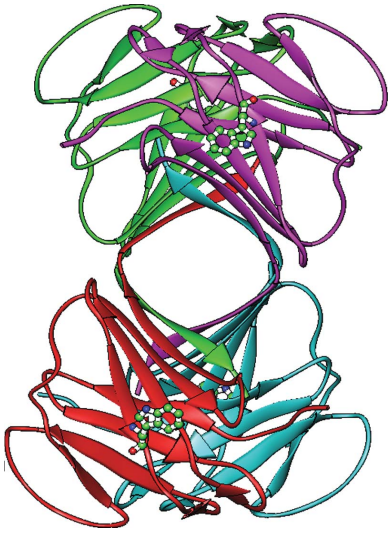

Proteins of the A-type lamin family, which consists of two members, lamin A and lamin C, are the major components of a thin proteinaceous filamentous meshwork, the lamina, that underlies the inner nuclear membrane. A-type lamins have recently become the focus of extensive functional studies as a consequence of the linking of at least eight congenital diseases to mutations in the lamin A/C gene (*LMNA*). This spectrum of pathologies, which mostly manifest themselves as dominant traits, includes muscle dystrophies, dilated cardiomyopathies, the premature aging syndrome Hutchinson–Guilford progeria and familial partial lipodystrophy (FPLD). The crystal structure of the lamin A/C mutant R482W, a variant that causes FPLD, has been determined at 1.5 Å resolution. A completely novel aggregation state of the C-terminal globular domain and the position of the mutated amino-acid residue suggest means by which the mutation may affect lamin A/C–protein and protein–DNA interactions.

1. Introduction

A most prominent feature in the cellular architecture of eukaryotic organisms is the nucleus, an organelle containing the genomic DNA. The boundary of the nucleus, the nuclear envelope, is contiguous with the endoplasmic reticulum and thus spatially conjugates the transcription and translation processes. The critical role of the nucleus in safeguarding and compacting the chromosomal DNA, together with its functional significance in regulating the process of cell division, underscore the demand for structural integrity of the nucleus in interphase cells while allowing dynamic disassembly and subsequent reassembly during mitosis. It has long been believed that the principal component of nuclear rigidity comes from the nuclear lamina: a meshwork structure composed of intermediate filament polypeptides that underlies the inner nuclear membrane. Although the role of the nuclear lamina in regulating the process of cell division has been established, it is only recently that other functional aspects of lamina biology have started to emerge in the light of some eight heritable diseases being linked to genetic defects in the lamin A/C gene (*LMNA*), which encodes one of the principal protein components of the nuclear lamina (Mounkes *et al.*, 2003).

The diversity of clinical pictures found in patients with selectively affected specific tissues, largely of mesenchymal origin, is caused primarily by different missense mutations in the *LMNA* gene. This observation has prompted several alternative models to explain how so many different diseases could be caused by mutations in the same almost ubiquitously expressed protein. According to one hypothesis, the so-called 'mechanical stress' model, the occurrence of a mutant lamin A/C chain, even on a background of the second *LMNA* allele producing a wild-type protein, may result in irregular binding properties of the functionally important lamin A/C dimers that are used as building blocks in lamina assembly. The resulting gross architecture of the nuclear lamina lacks structural rigidity and is vulnerable to

disintegration, particularly in cells that are subjected to mechanical stress or shearing force, such as muscle or cardiac tissues, or cells with active cytoskeleton dynamics, *e.g.* Schwann cells. This model explains the specific manifestations of mutagenesis in the otherwise ubiquitously expressed *LMNA* gene on striated and cardiac muscle tissues observed in patients with dilated cardiomyopathies and limb-girdle muscular atrophy (Shackleton *et al.*, 2000), but provides few hints regarding the cellular basis of the fat-tissue pathologies reported in familial partial lipodystrophy (FPLD) patients. The second concept, known as the 'aberrant gene-expression model', postulates a dominant effect of *LMNA* mutant isoforms on the transcription activity of isolated genes or signal transduction pathways that could ultimately influence tissue-maintenance processes or differentiation decisions of precursor cell pools. According to this hypothesis, the tissue specificity of the pathological outcome for a given *LMNA* mutation is determined by the expression patterns of potential binding partners and/or the cell type-specific consequences of impaired gene expression/signaling. To demonstrate the validity of the second concept, the protein structure of the LMNA globular C-terminal domain containing multiple mutations linked to at least five different diseases has been determined (Dhe-Paganon *et al.*, 2002; Krimm *et al.*, 2002). Intriguingly, several correlations between the structural basis of the location of a mutant amino acid and the resulting type of pathology have been demonstrated. For example, in the case of muscular dystrophy, associated mutations are distributed mostly in the protein core and are expected to cause global alteration of lamin A/C folding. On the other hand, all mutations causing FPLD in human patients are found within a small cluster of residues exposed on the surface and thus potentially altering the ectopic binding affinity (Cao & Hegele, 2000; Speckman *et al.*, 2000; Vigouroux *et al.*, 2001). These observations strongly suggest that perhaps a combination of both 'mechanical stress' and 'aberrant expression' models should be taken into account to provide a comprehensive explanation of LMNA-associated pathologies.

One of the residues that results in FPLD when mutated is Arg482. To further elucidate the molecular basis of the implications of structural changes in lamin A/C on the pathologies of fat tissue, we have determined the crystal structure of the C-terminal domain of the R482W mutant and analyzed the changes around the mutation site in detail.

2. Experimental procedures

2.1. Protein production and purification

The DNA encoding the R482W mutant of human lamin A/C (amino acids 435–552), extended at its N-terminus by a 6×His tag followed by a factor Xa cleavage site, was inserted into a pET41a(+) (Novagen) vector at the *Nde*I and *Eco*RI restriction sites. The protein was expressed in *Escherichia coli* BL21 Codon Plus cells and purified from the lysate by copper affinity chromatography (GE Healthcare Fast Flow Chelating Sepharose). The protein was concentrated to 2 ml and dialyzed in 50 m*M* HEPES pH 7.0 buffer containing 200 m*M* NaCl. The His tag was removed by overnight digestion with factor Xa [1:50(*w*:*w*), New England Biolabs] and the protein was applied onto the same copper column equilibrated with the above buffer. The flowthrough fraction containing R482W and factor Xa was concentrated to about 2 ml with Amicon Ultra 5K (Millipore), applied onto a HiLoad Superdex-75 (16/60) column (GE Healthcare) and the protein was eluted with 200 m*M* NaCl, 20 m*M* DTT, 50 m*M* HEPES pH 7.0 buffer. For crystallization, fractions containing the R482W mutant were pooled together and concentrated to 9.3 mg ml^{-1}.

Table 1
X-ray diffraction data and refinement statistics.

Values in parentheses are for the highest resolution shell.

X-ray data	
Resolution (Å)	45.0–1.5 (1.53–1.5)
Measured reflections	254359
Unique reflections	68652
Completeness (%)	82.2 (53.5)
$R_{\rm merge}$†	0.062 (0.37)
$I/\sigma(I)$	31.2 (4.2)
Refinement	
No. of non-H atoms	
Protein	3672
Waters	320
R factor‡	0.21 (0.33)
$R_{\rm free}$‡ (10% of data chosen randomly)	0.25 (0.37)
R.m.s.d.	
Bonds (Å)	0.018
Bond angles (°)	2.0
Ramachandran plot, residues in	
Most favored regions (%)	90.1
Additionally allowed regions (%)	9.9
Disallowed regions (%)	0.0

† $R_{\rm merge} = \sum_{hkl}\sum_i |I_i(hkl) - \langle I(hkl)\rangle| / \sum_{hkl}\sum_i I_i(hkl)$ ‡ *R* factor and $R_{\rm free} = \sum_{hkl} ||F_{\rm obs}| - |F_{\rm calc}|| / \sum_{hkl} |F_{\rm obs}|$.

2.2. Crystallization

The initial crystallization experiments were carried out using the Phoenix crystallization robotic system (Art Robbins Instruments, Sunnyvale, California, USA), employing the sitting-drop method. Small crystals were found in solution 14 of the Wizard I crystal screen (Emerald BioSystems, Bainbridge Island, Washington, USA) after one week. Crystals suitable for X-ray analysis were subsequently obtained by the hanging-drop vapor-diffusion method from a solution consisting of 0.9 *M* sodium citrate, 20 m*M* DTT, 100 m*M* sodium cacodylate pH 6.3. The unit-cell parameters were $a = 62.2$, $b = 84.0$, $c = 98.8$ Å in space group $P2_12_12_1$, with four molecules of the R482W mutant in the asymmetric unit.

2.3. Data collection, structure determination and refinement

Diffraction data were collected on the Southeast Regional Collaborative Access Team (SER-CAT) beamline ID-22 at the Advanced Photon Source, Argonne National Laboratory. Initially, crystals were cryoprotected for a few seconds in a solution containing 20% glycerol mixed with 80% well solution and were immediately frozen in a nitrogen stream at 100 K. Unfortunately, after this procedure the diffraction pattern exhibited a very high mosaicity (greater than 3°) and the crystals were annealed (Stevenson *et al.*, 2001) in cryoprotection solution for 4 min before final freezing. The annealing step improved both the mosaicity and the resolution, making it possible to collect diffraction data extending to 1.5 Å, although the diffraction pattern was still somewhat anisotropic. As a result of the anisotropy of diffraction, the completeness of the data is a little low (Table 1). The total rotation of the crystal around the spindle axis during data collection was 360°. The crystal structure was determined by the molecular-replacement method with the program *PHENIX* (Adams *et al.*, 2002) using the atomic coordinates of a wild-type lamin A/C fragment (PDB code 1ifr; Dhe-Paganon *et al.*, 2002) as a search model. After the positions of all four molecules of the mutant had been found, crystallographic refinement with the program *CNS* (Brünger *et al.*, 1998) against 1.5 Å resolution data was initiated with the application of noncrystallographic symmetry restraints. The final model was characterized by $R = 0.21$ and $R_{\rm free} = 0.25$, with r.m.s.d.s of bond lengths and angles from standard values of 0.018 Å and 2.0°, respectively (Table 1).

3. Results and discussion

3.1. Overall structure of the R482W mutant

The crystal structure of the R482W mutant of the globular tail domain (residues 435–552) of lamin was determined using the molecular-replacement method with the structure of the corresponding wild-type domain as an initial model (Dhe-Paganon *et al.*, 2002). The final refined model, based on data extending to 1.5 Å resolution, included four independent protein molecules (3672 non-H atoms) and 320 water molecules. Unlike the wild-type structure, in which residues 545–552 were disordered and could not be located in the electron-density map, all 118 amino-acid residues of the R482W mutant could be located unambiguously, thus allowing the tracing of the unique conformation of the C-terminal tail residues 545–552. Superposition of the C^{α} atoms of the wild-type protein with their counterparts in the R482W mutant showed that the two structures were very similar (Fig. 1). The r.m.s. deviation for residues 438–544 that can be seen in both structures was only 0.5 Å (Maiti *et al.*, 2004).

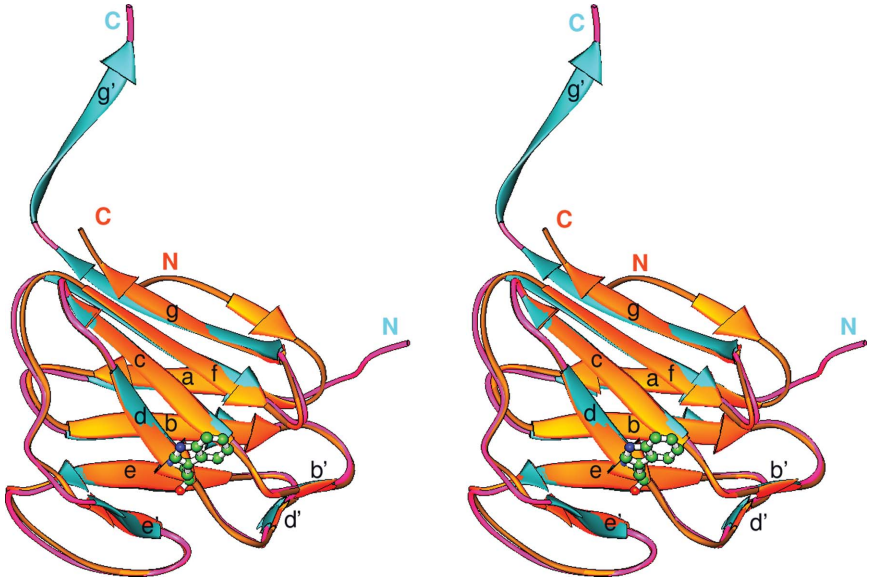

Figure 1
Stereo diagram of the superposition of the wild-type C-terminal domain of lamin A/C (PDB code 1ifr) with the R482W mutant. The wild-type protein is shown in orange, whereas the mutant is shown in cyan. The mutated side chain of residue 482 is shown as a ball-and-stick model, with carbon in green, oxygen in red and nitrogen in blue. The β-strands involved in the formation of the immunoglobulin fold are labeled as in the previously published structure of wild-type lamin (Dhe-Paganon *et al.*, 2002).

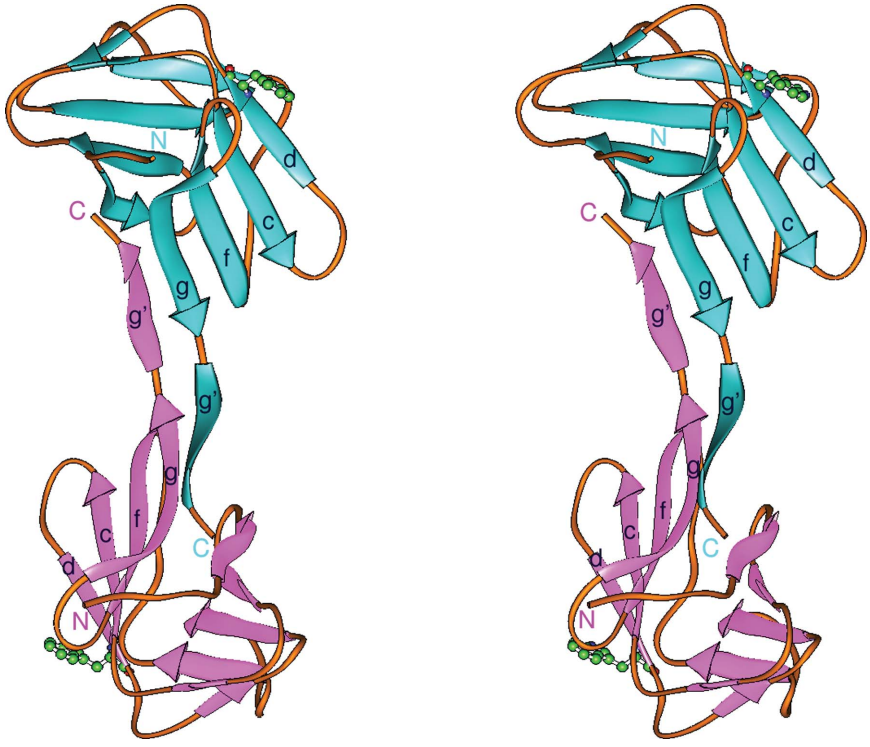

Figure 2
Stereo diagram of the dimer of the R482W mutant. The two monomers are shown in cyan and violet and the mutated side chain is shown as in Fig. 1.

The overall conformation of the molecule exhibits a characteristic new type of immunoglobulin fold (Bork *et al.*, 1994; Dhe-Paganon *et al.*, 2002) consisting of two four-stranded β-sheets (Fig. 1) packed in a compact β-sandwich that is very well preserved. The only major differences were found at the N- and C-termini of the protein. The amino-acid residues 432–437 located at the N-terminus of the construct expressing wild-type lamin A/C form the first β-strand in this structure. However, the first four residues (Gly432-Ser433-His434-Arg435) are cloning artifacts that do not belong to lamin A/C but originated from the type of construct that was utilized in producing recombinant protein. The sequence of the N-terminus of the R482W mutant protein contains just one residue Ser435 instead of Met435 as in the original sequence and residues 435–439 in the mutant structure form a short coil which is turned away from the main body of the protein. The C-terminal amino-acid residues 545–552 of the wild-type structure were disordered and could not be located in the electron-density maps, whereas in the mutant protein these residues create the additional β-strand g' (Fig. 1). This strand crosses the β-sheet made of strands *d*, *c*, *f* and *g* at an angle of about 90°. The site of the R482W mutation is located at the end of the β-strand *d*, with the side chain turned out towards the outer surface of the protein (Fig. 1).

3.2. New mode of aggregation of the R482W mutant

Although the crystals of both the wild-type and the mutant protein belonged to the same space group $P2_12_12_1$, the unit-cell parameters and crystal packing were completely different. The crystals of wild-type lamin A contained only a single protein molecule in the asymmetric unit, forming layers of molecules parallel to the crystallographic plane *ab* along the *c* axis. In the case of the R482W mutant the situation is quite different. Two crystallographically independent molecules of the mutant protein related by a noncrystallographic dyad interchange their β-strands g' (Fig. 2) to form an intercalated dimer. In both molecules strand g' is antiparallel to strand *g* and extends the β-sheet *d*, *c*, *f*, *g* from a four-stranded sheet to a five-stranded sheet. The surface area buried at the interface between the two molecules is 1596 Å^2. Two such dimers are also related by a noncrystallographic dyad perpendicular to the first one, forming the final tetramer (Fig. 3) present in the asymmetric part of the crystallo-

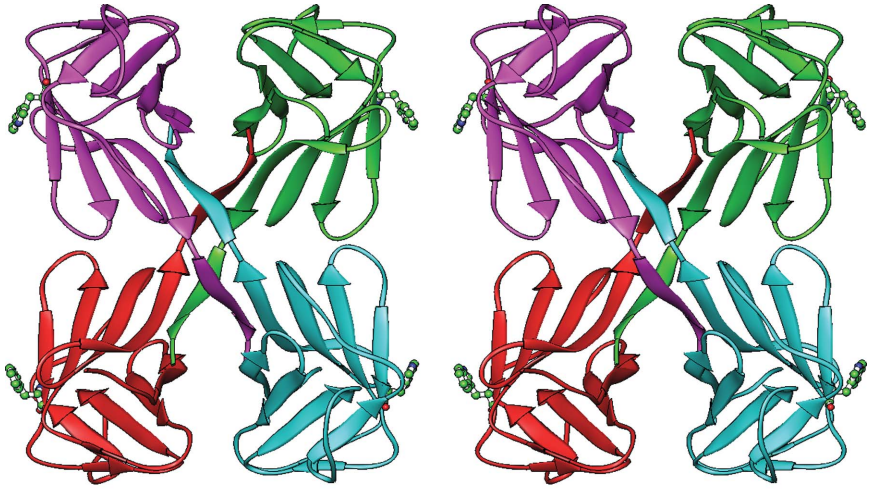

(*a*)

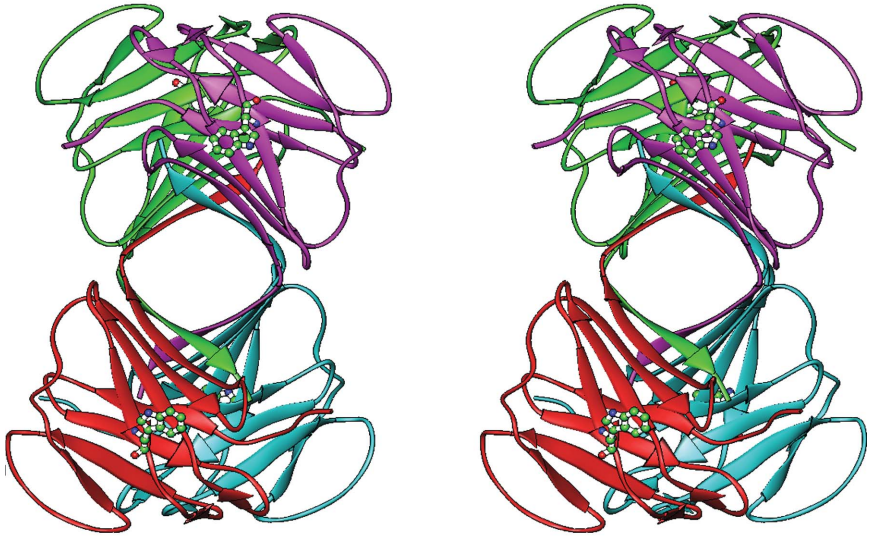

(*b*)

Figure 3
Stereo diagram of the tetramer of the R482W mutant. The individual monomers are shown in cyan, violet, green and red, respectively. The R482W mutation is shown in each monomer in ball-and-stick representation, with the same color code as in Fig. 1. (*a*) Front view of the tetramer. (*b*) Side view of the tetramer after 90° rotation.

graphic unit cell. The size of the tetrameric aggregate is ~50 × 50 × 40 Å, with a surface area buried in the interface between the dimers of 1746 Å^2. An interesting feature of the tetramer is the presence in its center of a 40 Å long channel made by the four β-sheets described above (Fig. 3). The shape of the channel resembles two funnels glued together by their narrow parts, with the narrow part of the channel made up of strands g and g' of all molecules participating in the formation of the tetramer. The tetramers are oriented in the crystal lattice in such a way that the axis of the channel is parallel to the crystallographic axis c, creating infinite channels in this direction in the crystal. The possible physiological role of the channel is not clear at this time, but its prominent features indicate that it may be important.

It is important to note that the formation of such a tetramer in the crystal structure of the wild-type protein (Dhe-Paganon *et al.*, 2002) would be impeded because of the position of the first N-terminal β-strand (432–437), which partially occupies the position of the intercalating strand g' of the noncrystallographic dimer of the R482W mutant. It is likely that such a conformation of the N-terminus occurs because of amino acids 432–435, which are derived from the cloning vector; in the absence of these residues the conformation of the wild-type protein in this area could be different.

3.3. Position and role of the R482W mutation in protein–protein/DNA interactions

The side chain of Trp482 is located on the surface of the protein and does not interact with any other side chain either in the dimer or in the tetramer. It is symmetrically positioned at the top and the bottom of the entry to the above-mentioned channel (Fig. 3), in proximity to a positively charged region formed by the side chains of Arg439, Lys470, Lys486, Lys515 and Arg527. Since the structure of the mutant protein does not vary as a consequence of the amino-acid substitution (Fig. 1), it is very likely that the influence of the R482W mutation on the functional properties of the protein may involve perturbation of the positive charge at the surface of lamin A/C, preventing interactions with its putative biological partner(s) at the inner nuclear membrane or interactions with DNA. It has been shown (Stierlé *et al.*, 2003) that the fragment 411–553 of lamin A/C, which includes the nuclear localization signal (NLS) 414–427, can bind nonspecific DNA sequences with micromolar affinity. The presence of both the NLS and an Ig-like domain proved to be important for binding; furthermore, the mutations in the latter that are responsible for FPLD decrease the affinity of the protein for DNA. It has also been suggested that protein–DNA binding could take place upon formation of a covalent dimer in which two monomers are bound through an intermolecular Cys522–Cys522′ disulfide bridge, despite the fact that all events occur inside the living cell in the cytosol and nucleoplasm environment under reducing conditions. Although the formation of such a disulfide bond might be possible, we have not seen any indication of it in the structure of the mutant lamin as crystallization was carried out in the presence of 20 mM DTT. In other words, the dimeric structure shown in Fig. 2 and the tetrameric structure shown in Fig. 3 exist under reducing conditions. The removal of DTT from protein solution concentrated to more than 1.0 mg ml^{-1} led to the formation of covalent dimers through the creation of disulfide bridges between Cys522 of neighboring molecules although, as shown by size-exclusion chromatography (unpublished data), the protein was still a mixture of dimers and monomers. Cys522, the only cysteine present in this domain of lamin A/C, was found in the crystal structure of the R482W mutant in a sulfinic acid form (Fig. 4). This oxidation occurred after the crystal had formed.

3.4. Is an allosteric effect caused by R482W or R482Q mutations possible?

We have analyzed what would happen to the wild-type structure of lamin A/C upon an R482Q mutation, which similarly to R482W also causes FPLD (Cao & Hegele, 2000). Since the side chain of the mutated residue is located on the surface of the protein at the entry of the 40 Å long channel and many properties of the tryptophan side chains match those of glutamine, it is very likely that both the dimer (Fig. 2) and tetramer (Fig. 3) of the R482Q mutant will be the same as those of the R482W mutant.

Both R482W and R482Q mutations may lead to an allosteric effect, allowing the repositioning of the C-terminal β-strand g' (Fig. 1) in a

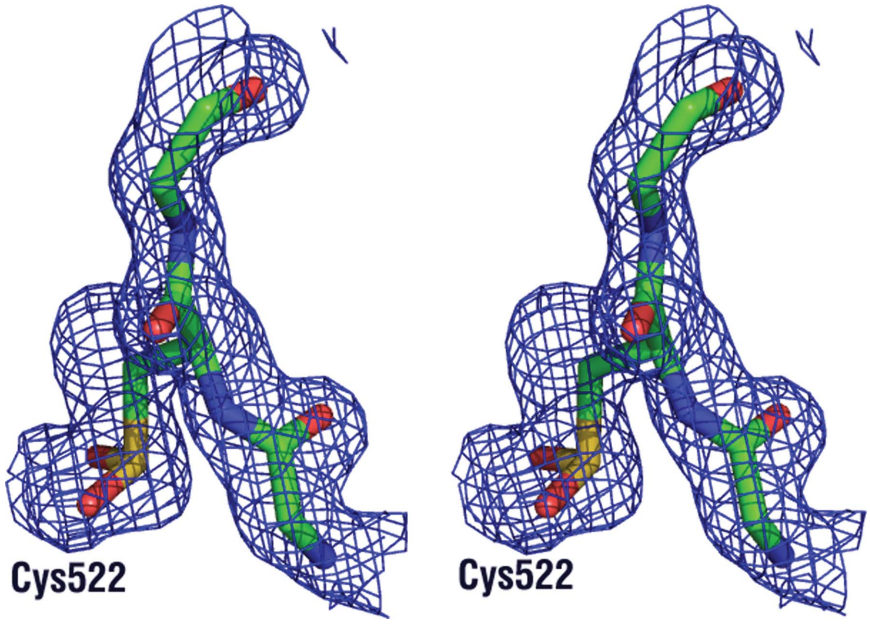

Figure 4
Stereo diagram of the $2F_o - F_c$ electron density (contoured at 1.5σ) superimposed on a stick model of the oxidized Cys522, showing the presence of sulfinic acid.

completely different position from that in the wild-type structure and causing a novel aggregation state of the mutant protein. Such conformational changes resulting in a completely new aggregation state caused by just a single mutation have been reported previously for other protein structures. A good example is provided by the structure of porphobilinogen synthase (Breinig *et al.*, 2003), in which the mutation F12L initiated the rearrangement of the N-terminal β-strand, which in turn initiated an octamer–hexamer transition of the aggregation state. As a result, the kinetic properties and activity profile of the mutated porphibilinogen synthase changed significantly.

As mentioned above, the cloning artifacts residues 432–435 of the wild-type structure could have prevented the formation of a dimer similar to that of R482W and it is obvious that in order to clarify the question of whether the wild-type protein can or cannot form this type of aggregate we need a wild-type structure with a native N-terminus. However, in the absence of this information, speculation that R482W or R482Q mutations may cause conformational change leading to a completely new aggregation state remains possible.

It is important to remember that the protein that we have studied is only part of a much larger structural protein and for this reason any conformations or aggregation states either in solution or in the solid phase are equally relevant or irrelevant to its biological role. The tetramer of R482W that we have found here has never been observed previously either in crystals of wild-type protein or in solution in NMR studies. However, it exists and has a unique tetramer structure under reducing conditions and thus may bring us to an improved understanding of how nuclear lamina is formed and functions.

This project was supported by the Intramural Research Program of the NIH, National Cancer Institute, Center for Cancer Research and with Federal funds from the National Cancer Institute, NIH under Contract No. NO1-CO-12400. The content of this publication does not necessarily reflect the views or policies of the Department of Health and Human Services, nor does the mention of trade names, commercial products or organizations imply endorsement by the US Government.

References

Adams, P. D., Grosse-Kunstleve, R. W., Hung, L.-W., Ioerger, T. R., McCoy, A. J., Moriarty, N. W., Read, R. J., Sacchettini, J. C., Sauter, N. K. & Terwilliger, T. C. (2002). *Acta Cryst.* D**58**, 1948–1954.

Bork, P., Holm, L. & Sander, C. (1994). *J. Mol. Biol.* **242**, 309–320.

Breinig, S., Kervinen, J., Stith, L., Wasson, A. S., Fairman, R., Wlodawer, A., Zdanov, A. & Jaffe, E. K. (2003). *Nature Struct. Biol.* **10**, 757–763.

Brünger, A. T., Adams, P. D., Clore, G. M., DeLano, W. L., Gros, P., Grosse-Kunstleve, R. W., Jiang, J.-S., Kuszewski, J., Nilges, M., Pannu, N. S., Read, R. J., Rice, L. M., Simonson, T. & Warren, G. L. (1998). *Acta Cryst.* D**54**, 905–921.

Cao, H. & Hegele, R. A. (2000). *Hum. Mol. Genet.* **9**, 109–112.

Dhe-Paganon, S., Werner, E. D., Chi, Y. I. & Shoelson, S. E. (2002). *J. Biol. Chem.* **277**, 17381–17384.

Krimm, I., Ostlund, C., Gilquin, B., Couprie, J., Hossenlopp, P., Mornon, J. P., Bonne, G., Courvalin, J. C., Worman, H. J. & Zinn-Justin, S. (2002). *Structure*, **10**, 811–823.

Maiti, R., Van Domselaar, G. H., Zhang, H. & Wishart, D. S. (2004). *Nucleic Acids Res.* **32**, W590–W594.

Mounkes, L., Kozlov, S., Burke, B. & Stewart, C. L. (2003). *Curr. Opin. Genet. Dev.* **13**, 223–230.

Shackleton, S., Lloyd, D. J., Jackson, S. N., Evans, R., Niermeijer, M. F., Singh, B. M., Schmidt, H., Brabant, G., Kumar, S., Durrington, P. N., Gregory, S., O'Rahilly, S. & Trembath, R. C. (2000). *Nature Genet.* **24**, 153–156.

Speckman, R. A., Garg, A., Du, F., Bennett, L., Veile, R., Arioglu, E., Taylor, S. I., Lovett, M. & Bowcock, A. M. (2000). *Am. J. Hum. Genet.* **66**, 1192–1198.

Stevenson, C. E. M., Mayer, S. M., Delarbre, L. & Lawson, D. M. (2001). *J. Cryst. Growth*, **232**, 629–637.

Stierlé, V., Couprie, J., Ostlund, C., Krimm, I., Zinn-Justin, S., Hossenlopp, P., Worman, H. J., Courvalin, J. C. & Duband-Goulet, I. (2003). *Biochemistry*, **42**, 4819–4828.

Vigouroux, C., Auclair, M., Dubosclard, E., Pouchelet, M., Capeau, J., Courvalin, J. C. & Buendia, B. (2001). *J. Cell Sci.* **114**, 4459–4468.